Photoinduced Surface Potential Change of Bacteriorhodopsin Mutant D96N Measured by Scanning Surface Potential Microscopy

Ida Lee,*,† Elias Greenbaum,‡ Stephen Budy,§ Jason R. Hillebrecht,|| Robert R. Birge,|| and Jeffrey A. Stuart*,§,⊥

Department of Electrical and Computer Engineering, University of Tennessee, Knoxville, Tennessee 37996-2100, Chemical Science Division, Oak Ridge National Laboratory, Oak Ridge, Tennessee 37831-6194, W. M. Keck Center for Molecular Electronics and Department of Chemistry, Syracuse University, Syracuse, New York 13244, and Department of Chemistry, University of Connecticut, Storrs, Connecticut 06269

Received: June 2, 2005; In Final Form: January 19, 2006

We report the direct measurement of photoinduced surface potential differences of wild-type (WT) and mutant D96N bacteriorhodopsin (BR) membranes at pH 7 and 10.5. Atomic force microscopy (AFM) and scanning surface potential microscopy (SSPM) were used to measure the BR membrane with the extracellular side facing up. We present AFM and SSPM images of WT and mutant D96N in which the light-dark transition occurred in the mid-scan of a single BR membrane. Photosteady-state populations of the M state were generated to facilitate measurement in each sample. The photoinduced surface potential of D96N is 63 mV (peak to valley) at pH 10.5 and is 48 mV at pH 7. The photoinduced surface potential of WT is 37 mV at pH 10.5 and ∼0 at pH 7. Signal magnitudes are proportional to the amount of M produced at each pH. The results indicated that the surface potentials were generated by photoformation of surface charges on the extracellular side of the membrane. Higher surface potential correlated with a longer lifetime of the charges. A mechanistic basis for these signals is proposed, and it is concluded that they represent a steady-state measurement of the B2 photovoltage.

Introduction

Bacteriorhodopsin (BR) is a 248 amino acid integral membrane protein found in the purple membrane of *Halobacterium salinarum* (aka *Halobacterium halobium*) that acts as a light to chemical energy transducer by pumping protons across the cell membrane in response to sunlight.[1] The resulting electrochemical gradient can be as large as 1 pH unit and is used by the cell to fuel an F0/F1 ATPase. BR has seven trans-membrane α-helices that make up the protein's secondary structure. An all-trans retinal chromophore covalently bound via a Schiff base linkage to Lys-216 mediates light absorption centered at 570 nm, which drives the protein through a series of photochemical and thermal intermediates typically referred to as the photocycle. The purple membrane enables the organism to act as a facultative anaerobe by switching from respiratory oxidative phosphorylation to photosynthesis as a means of energy production when the dissolved oxygen concentration drops below the threshold level. Absorption of light by the chromophore causes a nearly instantaneous (femtoseconds) shift of negative charge that initiates a rapid (picoseconds) all-trans to 13-cis photoisomerization. The complex photochemical cycle that follows involves several sequential intermediate states denoted as K, L, M, N, and O, as shown in Figure 1 (from ref 2). The photocycle occurs in approximately 10 ms at room temperature and completes with the reformation of the initial BR state.[3] The photocycle intermediates are formed as a function of modulations of the electrostatic interactions between the retinal chromophore and surrounding amino acids. Formation of the K state is often referred to as the primary event, i.e., the photoisomerization of the all-trans retinal chromophore to 13-cis. The remaining intermediates are formed thermally and facilitate proton translocation from the cytoplasmic to extracellular side of the membrane through a series of deprotonation and reprotonation events along the proton pathway channel. Finally, the protein is reset back to the BR resting state with the decay of the O-intermediate and the consequent reisomerization of the retinal chromophore.

Over the past two decades, BR has received much attention for biomolecular electronic device applications.[4] Device applications fall into two categories: those that rely on the photochromic properties of the protein and those that utilize the photovoltaic (photoelectric) effect. Although the native protein can be used in various devices, chemical or mutagenic modification is often required for optimized performance. One of the first to be explored in this vein was the mutant D96N, which has a longer M-state lifetime due to the replacement of aspartic acid (Asp-96) by asparagine (Asn-96).[5] This protein continues to be utilized for holographic applications.[6−8] Furthermore, D96N has proven to be a particularly important mutant for biophysical studies of the protein, having made possible high-resolution crystallography studies of the M state.[9−11] Manipulation of the photokinetic behavior of the D96N mutant can be accomplished easily by chemical modification of its environment; charge motions inside the protein are strongly pH dependent and a longer M-state lifetime is observed with

* E-mail: ilee1@utk.edu (I.L.), corresponding author for SSPM related questions; jeffrey.stuart@uconn.edu (J.A.S.), corresponding author for BR related questions.

† University of Tennessee.

‡ Oak Ridge National Laboratory.

§ Syracuse University.

|| University of Connecticut.

⊥ Present address: Department of Chemistry, University of Connecticut, Storrs, Connecticut 06269.

10.1021/jp052948r CCC: $33.50
Published on Web 04/28/2006

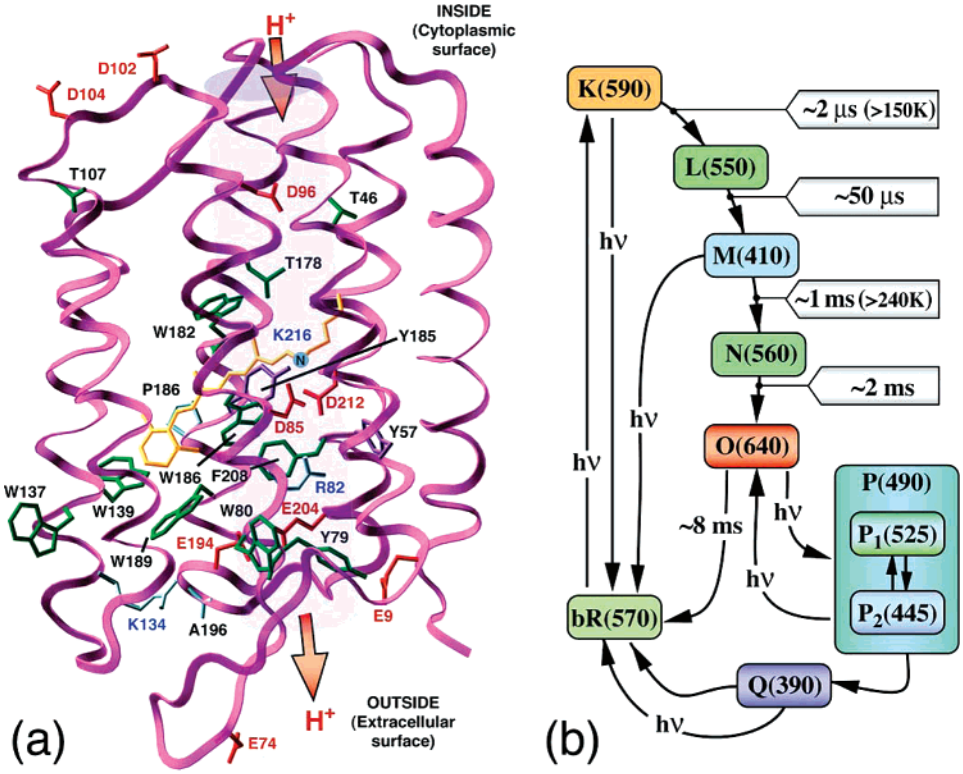

Figure 1. Structural schematic of (a) bacteriorhodopsin and (b) photocycle.

increasing pH.[12] The ability to drive large amounts of the protein into the M state at room temperature has facilitated a large number of studies focusing on this key BR photocycle intermediate.

Both the M and O intermediates are strongly affected by pH; this is not surprising considering that proton uptake from the cytoplasm occurs during the N to O transition and proton release to the extracellular side occurs during the M state. The M state is particularly susceptible, and increasing the pH can significantly prolong the lifetime of this intermediate by inhibiting N formation. Formation of the M state is characterized by a shift in the absorption maximum from 570 to 410 nm, deprotonation of the Schiff base linkage, and protonation of the primary counterion, Asp-85. The M to N transition depends on reprotonation of the Schiff base linkage by a proton donated from Asp-96. The M state is largely understood to consist of multiple forms, most commonly denoted as M_1 and M_2. These forms represent equilibrium stages of the various transitions in the M state, including the deprotonation of the Schiff base (M_1), reprotonation of Asp-85 and protein reorganization as a response to M_1 (reorientation of the Schiff base from facing the extracellular direction to the cytoplasmic direction during the M_1 to M_2 transition), proton release to the extracellular side (M_2 to M_2'), and further protein reorganization in preparation for the proton transfer between Asp-96 and the Schiff base characterized by the M_2' to N transition.[9,11,13−16]

On a molecular level, several salient events characterize the M state. The proton transfers that result in both formation and decay of the M state have been known for some time. During formation of the M state, the Schiff base donates its proton to one of the primary counterions, Asp-85 (M_1). After Asp-85 protonation, the chromophore relaxes to a full 13-cis configuration, repositioning the Schiff base toward the cytoplasmic side of the membrane and Asp-96. This transition is a prerequisite for Schiff base reprotonation from Asp-96 and has often been postulated as the protonation switch that enables unidirectional proton transport.[13,16,17] Proton transfers throughout the photocycle are driven by shifts in the pK_a values of the various participant functional groups, including Asp-85 and Asp-96, the Schiff base, and the proton release group on the extracellular surface.[18] The latter most probably is composed of two glutamate residues (194 and 204) and a hydrogen-bonded network of water molecules.[19−24] Various authors have theorized for some time that the pK_a values of Asp-85 and Glu-204 are somehow coupled,[25] although a mechanism has only recently been made possible by crystallographic studies of the trapped M state.[10,11,26] It seems the mechanism that drives proton transfer is mediated by the positively charged Arg-82—the arginine amidinium group shifts from close proximity to the Schiff base and Asp-85 (toward the cytoplasmic surface) to an orientation favoring proximity to Glu-204 and the extracellular surface.[11,27] As a consequence, Glu-204 changes position to favor enhanced hydrogen bonding with Arg-82 while pulling away from Glu-194.[11] Reorientation of the arginine-82 amidinium group facilitates extracellular proton release, occurs during the late phase of the M state (M_2), and is most likely driven by the protonation of Asp-85.[27]

The BR photocycle is typically monitored by following the time-resolved modulation of the visible absorption profile. However, BR photoactivity can also be tracked as a function of light-induced voltage and current changes. Such charge movements range in time scale from the picosecond to the millisecond regime and are characterized by three phases in oriented samples, denoted as B1, B2, and B3,[28] as shown in Figure 2. The fast B1 component of the photovoltage consists of a picosecond time scale negative voltage spike.[28] The B2 component follows, reversing signal polarity, and lasting ~200 microseconds before the onset of B3, which is essentially a millisecond time-scale decay of B2. The biophysical basis for the origins of these signals is somewhat ambiguous, although B1 has generally been attributed to K-state formation and B2 is believed to be associated with the L to M transition;[28,29]

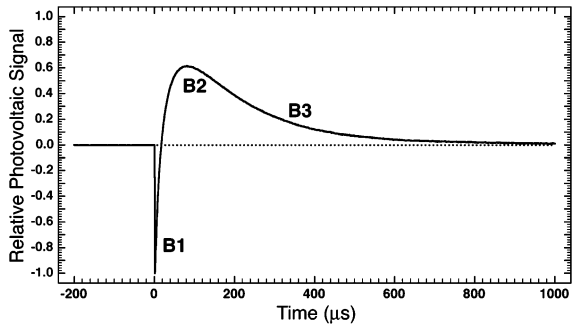

Figure 2. Bacteriorhodopsin photoelectric effect. See text for details.

however, few mechanistic details for either component (or B3) have been proposed. El-Sayed and co-workers observed that in contrast to B1 and B2, the polarity of B3 is independent of protein orientation; the signal was attributed to the formation of a transient capacitor between ITO electrodes as a function of BR-facilitated proton pumping.[30] A recent paper by Xu and co-workers attributes the B1 component to partial chromophore isomerization and a coupled motion of Arg-82 toward the primary counterions, Asps 85 and 212, upon formation of the K state.[31]

The surface of BR membranes has been imaged previously by electron cryomicroscopy at a resolution of 0.3 nm.[32] The amino acids responsible for proton transduction have been identified through numerous site-directed mutagenesis studies, as well as through more recent crystal structures (see references cited above). The BR crystal structure at <0.1 nm resolution of an early protein photocycle intermediate has been obtained by X-ray diffraction.[33] Within the past few years, several high-resolution crystal structures of BR have become available, and more recently, structures of several trapped intermediates have also been published.[10,13,16,26,27,34] Despite the wealth of information available by means of genetic and crystallographic studies, measurements of the photoelectric response of BR surface properties are often contradictory and their underlying mechanisms have remained elusive. The ability to directly measure photoinduced surface potentials can reveal important characteristics of the protein. The surface potentials of BR crystals have been measured in $NaNO_3$ solution at various pH values using atomic force microscopy (AFM) with a silica sphere attached to the probe.[35] Analysis of the force curves suggested that the surface charge of BR crystals under the protein surface remained constant during the approach of the silica colloid probe. Electrostatic force microscopies, such as the Kelvin probe force microscope (KFM),[36] Maxwell stress microscope (SMM),[37] and scanning surface potential microscope (SSPM),[38] have been used to study the molecular orientation and photoinduced charge separation in Langmuir−Blodgett (LB) films.[39] Previously, we used the SSPM technique to obtain quantitative values of the light-induced photovoltage at nanometer resolution from single photosynthetic reaction centers that were immobilized on gold.[40] This technique can also be used to study electrostatic potentials at the air−liquid interface.[41,42] We report here the first SSPM measurement of photovoltages from immobilized BR wild type and BR D96N at pH 7 and 10.5.

Experimental Section

The substrate used for the experiments was muscovite mica, which is composed of layered crystals with cleavage planes that are atomically flat over several hundred μm^2. The basic muscovite structure in the vertical direction is composed of repetitive potassium ions sandwiching a layer of aluminum ions in octahedral coordination (surrounded by six oxygen ions), which in turn are sandwiched between two layers of silicon ions in tetrahedral coordination (surrounded by four oxygen ions). The surface charge of muscovite is negative in the entire studied pH range.[43] The electrostatic interactions play an important role in the adsorption and binding of charged biomolecules. In the case of negatively charged structures and molecules such as the purple membrane and DNA, it is necessary to carry out adsorption at high salt concentrations to screen electrostatic repulsion and permit adsorption by attractive van der Waals interactions. Muller et al. have investigated the adsorption density of purple membrane as a function of salt concentration and pH.[44] In the case of the monovalent salt KCl, the maximum adsorption density was achieved with an electrolyte concentration of 50 mM. Further increase of salt concentration, up to 300 mM, did not result in a higher adsorption density. The pH of the buffer solution is an additional factor that can influence the adsorption of purple membrane. However, at salt concentrations of more than 50 mM, a variation of pH did not influence the adsorption density.

The buffer used for these studies was 100 mM potassium chloride (KCl), 10 mM Trizma, pH 7 and 100 mM KCl, 50 mM Trizma, pH 10.5 for BR wild-type (BR-WT) and BR D96N (BR-D96N) at a concentration in the range of $2-5$ μg/mL. This buffer was used to orient and adhere the BR sample onto the atomically flat mica surface. The two surfaces of the BR membrane, the extracellular and cytoplasmic surfaces, have different surface morphologies. The extracellular surface appeared "cracked" whereas the cytoplasmic surface appeared pitted.[45] All of our 2-dimensional AFM images (not shown) have fine cracks on the surface. This indicated that all the BR membranes shown here are oriented with the extracellular surface on top. Muller et al. have distinguished the cytoplasmic and extracellular surface of purple membrane on mica at pH 9.2 by immuno-atomic force microscopy.[46] They found $\sim$70% of the membranes oriented with the extracellular surface on top.

In the experiments reported here, the cytoplasmic side of BR was attached to the mica surface. The protein was resuspended in ultrapure deionized water and centrifuged (12 000 rpm for 15 min) to remove aggregates and contaminants. The last dilution was made with the buffer. The diluted solution (30 μL) was applied to freshly cleaved mica (9.9 mm, Ted Pella, Inc., Redding, CA) and allowed to sit for 15−30 min. The surface was carefully rinsed with buffer (250 μL) and last with ultrapure deionized, sterile water (250 μL). The samples were dried with nitrogen (N_2) for 2−5 min and then sealed inside an ultraclean container prior to imaging. It should be noted that under these conditions, the pH experienced by the protein is not expected to change significantly from that of the buffer. The critical residue for M-state decay is D96, which must be deprotonated to prolong the M-state lifetime. In the BR resting state, D96 is buried in a hydrophobic cavity located closer to the cytoplasmic surface; proton transfer to the Schiff base (a distance of $\sim$10 Å) is facilitated only after BR activation by light, when a transient hydrogen-bonding network is thought to be formed as a result of structural changes in the protein.[47−51] As detailed above, purple membrane patches are oriented such that the cytoplasmic surface is bound to the mica in these experiments, thereby further insulating D96 from solvent-induced pH changes. Given these parameters, it is unlikely that the pH experienced by D96 was changed to any significant extent by the sample preparation procedures outlined above.

A modified Nanoscope IIIa (Digital Instruments) was used to study the surface potentials. The measurements were per-

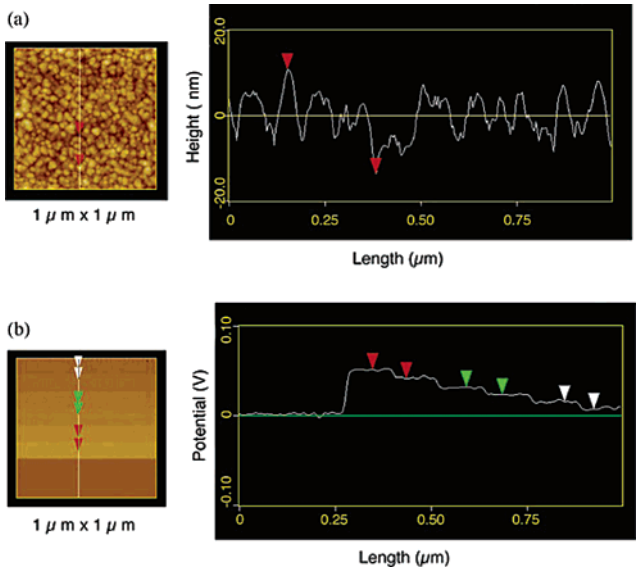

Figure 3. Images on the left are dual images that employed (a) tapping mode AFM for topographic imaging and (b) lift-mode SSPM for voltage imaging. Tapping mode atomic force microscopy (AFM) surface topography of a single line was first scanned and recorded followed immediately by a second scan of the recorded line for electric potential measurement (SSPM) at a set height of 30 nm away from the sample surface, using the built-in lift-mode feature. The locations of cross-sections (the figures at the right) taken are indicated by a line at the left images. (a) Vertical distance between the two red pointers is 27 nm. (b) Potential difference between the two pointers in red is 10.4 mV, green is 8.9 mV, and white is 8.5 mV.

formed in an environmental chamber with ultrapure nitrogen gas (99.9997%) at a relative humidity (RH) of 65−70%. The experiments were performed in high humidity because studies have shown that the internal water molecules in BR participate in proton pumping functionality.[52] First, the surface topography was measured by recording a line trace with the AFM operating in tapping mode. By use of the built-in lift-mode feature, the surface topography trace was followed immediately by a second, spatially elevated, trace for measurement of the electric potential at a height of 30 nm above the sample surface. The surface topography and corresponding SSPM map were recorded on a raster-by-raster basis with alternating sequential scans at a scan rate of 1 Hz; 265 lines were used to form two-dimensional images. Illumination of the BR membrane was achieved using an external diode laser in the wavelength range 600−1550 nm. Our images consist of WT and D96N in which the light-dark transition occurred in the mid-scan of a single BR membrane. The mica substrate with BR membrane was attached to a metal disk, which was held at ground potential (0 V).

The SSPM was calibrated with specially prepared surface structures in which gold was sputtered on ultraflat cover-glass slides. Various DC step voltages of 10 mV interval provided a constant voltage source correlated with the electric-potential image map of the structures obtained with SSPM. As shown in Figure 3a, the AFM image of the calibration sample has particle-like structure of ∼20 nm in height. The roughness of the gold grain is similar to that of the BR membrane: smaller than 30 nm. As such, crosstalk is not a problem. Figure 3b is the corresponding SSPM measurement of the same area shown in Figure 3a. As shown in Figure 3a,b, the AFM image was not influenced by the voltage applied on the sample because steps of voltage were not observed, and the SSPM image did not shown any surface structure. We thus rule out the possibility of crosstalk between topography and surface potential. The standard deviation from the calibration data is 0.79 mV. The calibration data indicated a minimum detection limit of ∼1 mV. As described previously,[40] a long and slender but slightly blunt SSPM probe was used. With this probe design (apex radius of 100 nm), the measured potential is approximately equal to the actual potential (error ≤ 5%).[53]

Theory and Modeling

For theoretical and mathematical modeling, electrostatic contour maps were generated using the 2.0 Å crystal structures of the BR variant, D96N, in both the resting (1C8R) and the late M state (1C8S) of the photocycle.[10] Unfortunately, at this time no corresponding M-state structure has been reported for the wild-type protein, so the corresponding calculations were not possible; however, we expect that the structure of the M state in the D96N variant will be very similar to that observed in the native protein because the chromophore binding site and the nearby ionic residues are all identical. Because the 1C8S structure is missing residues at positions 154 → 175 and 223 → 231, the corresponding amino acids were omitted from the 1C8R structure. The valence for Phe-153, Asn-176, and Ile-222 were then verified to maintain consistency for both structures.

Hydrogen atoms were added to both structures, and charges were assigned to Thr-5 (+), Arg-82 (+), Asp-85 (−), Glu-194 (−), Asp-212 (−), and Lys-216 (+) for 1C8R. The charge assignments for 1C8S were consistent with 1C8R, with the exception of Asp-85 and Lys-216. During the M state, the translocation of a proton from the Schiff base to Asp-85 requires that Asp-85 and Lys-216 be neutralized in 1C8S. All of the remaining amino acids were neutralized, and the overall charge of both structures was zero.

The hydrogen atoms of each structure were minimized using the PM3 Hamiltonian within MOZYME.[54] MOZYME, a version of MOPAC, is a module of CAChe 6.1.1 used to minimize the geometry of large systems, specifically proteins. The PM3 Hamiltonian was chosen because it provides a more realistic description of water molecules and of retinal chromophores, relative to the AM1.[55−57] All non-hydrogen atoms were locked during the entire minimization, and the calculations were terminated upon achieving a self-consistent field criterion (SCFCRT) equal to 1.0. Due to the limitations of MOZYME, the calculations were broken up into a series of abbreviated (100 iterations) calculations. Restricting MOZYME calculations to no more than 200 cycles prevents drastic changes in the geometry of the protein from occurring during the calculation.[56] The MOZYME calculations were terminated and restarted until both 1C8R and 1C8S achieved convergence at 386 and 364 total iterations, respectively. Electrostatic difference maps were generated using Anamol, a program available via email from R. R. Birge (rbirge@uconn.edu).

Results and Discussion

Our AFM images indicated that all the BR membranes, WT and D96N at pH 7 and 10.5, were ∼5 nm in height and 0.5−1.0 μm in diameter. Previous studies have shown that the lattice spacing of the hexagonal unit cell containing the BR trimer is ∼6 nm.[54] For our application, to ensure the accuracy of the surface potential measurements, a probe of ∼100 nm was used for both AFM and SSPM images. Thus, the roughness shown in our AFM images did not represent the BR unit cell because the radius of our cantilever probe was much bigger than the BR unit cell. The resolution of our AFM images is not as good as AFM images that use ultrasharp tips. However, in our

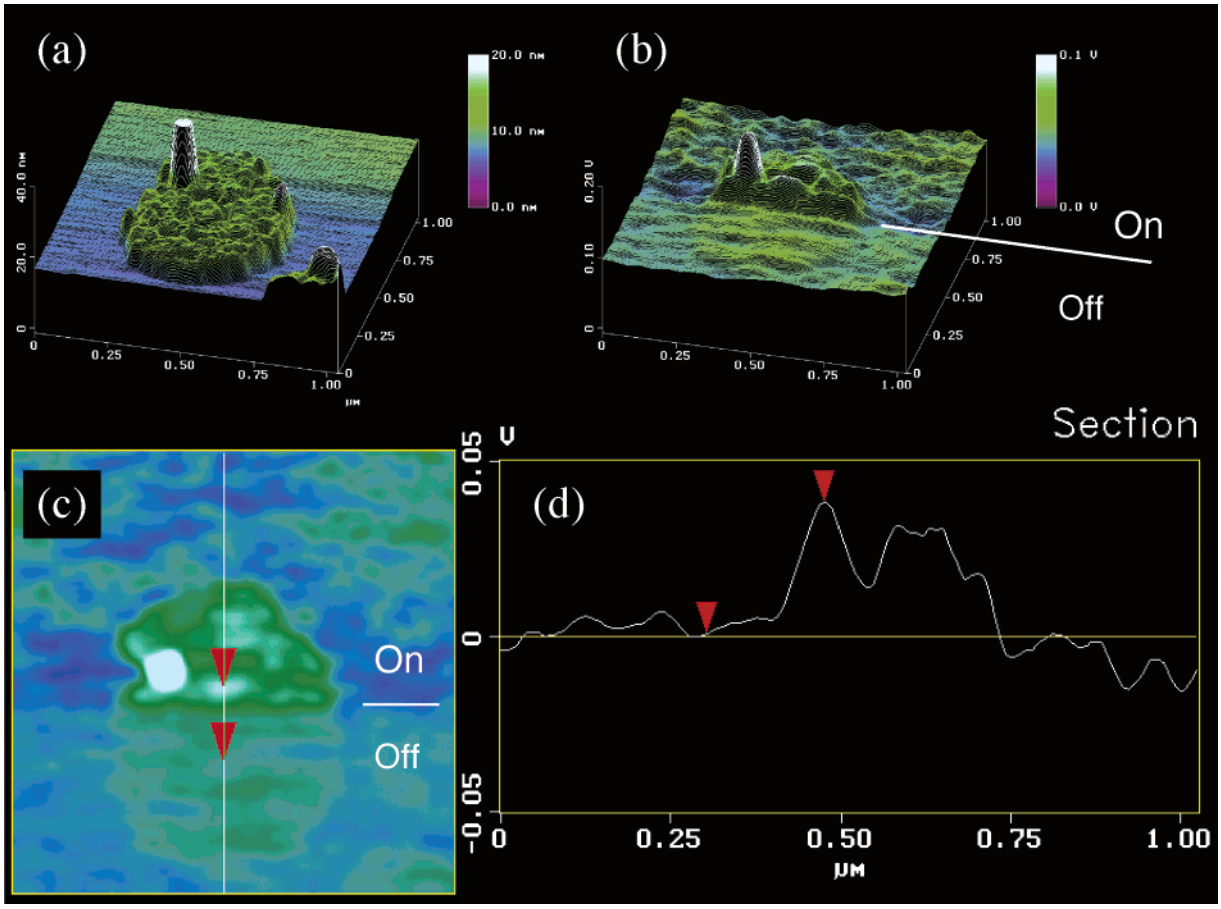

Figure 4. WT BR at pH 10.5: (a) 3-dimensional AFM topographic image; an abnormal topography (a tall spike) can be observed in the upper-left-hand corner and is avoided for SSPM cross section measurement, (b) corresponding SSPM surface potential image. The laser light was on in the first half of the scan. The light was then turned off in the mid scan, as indicated in (b) and (c), and stayed off during the rest of the scan, (c) two-dimensional SSPM image of (b), and (d) value of the surface potential at the cross section in (c). In graph (d), the 0 μm is at the bottom of the graph (c) and that is light-off on mica. The first pointer is at light-off on BR WT, and the second pointer is at light-on on BR WT. The potential then falls to ~0 V (at around 0.75 μm mark) on light-on mica surface. The vertical distance between the two pointers, which corresponds to the surface potential difference between light on and light off for BR WT, was 37 mV.

experiments, AFM images were used merely as a reference for the corresponding SSPM images. This is necessary to avoid erroneous SSPM values caused by occasional abnormal topography, one example of which is illustrated in the upper-left-hand corner of Figure 4a. As described in our Eperimental Section, Muller et al. have distinguished the cytoplasmic and extracellular surface of purple membrane on mica at pH 9.2 by immuno-atomic force microscopy. They found ~70% of the membranes oriented with the extracellular surface on top. Our observation of the membrane orientation by AFM is statistically consistent with Muller's result. Figure 4a is the 3-dimensional AFM topographic image of WT-BR at pH 10.5, and Figure 4b is the corresponding SSPM surface potential image. The laser light was on in the first half of the scan. It was then turned off in mid scan, as indicated in Figure 4b,c, and stayed off during the rest of the scan. Figure 4c is the two-dimensional SSPM image of Figure 4b. Figure 4c indicates the location where the cross section and the two pointers were taken. Figure 4d is a plot of the surface potentials at the cross section in Figure 4c. The vertical distance between the two pointers, which corresponds to the surface potential difference between light on and light off for WT-BR, was 37 mV. The surface potential measurements in this study are light-on BR potential versus light-off BR potential. The same measurements were performed on BR D96N at pH 7.3 and pH 10.5. Figure 5a illustrates the AFM topographic image of BR D96N at pH 7.3, and Figure 5b shows the corresponding SSPM surface potential image. Figure 5d is the surface potential at the cross section indicated in Figure 5c and the vertical distance between the two pointers, which indicated light-on vs light-off for BR D96N at pH 7.3, was measured to be 48 mV. Figure 6a is the AFM topographic image of BR D96N at pH 10.5 and the corresponding SSPM surface potential image is shown in Figure 6b. The surface potential at the cross section indicated in Figure 6c is shown in Figure 6d, and the vertical distance between the two pointers, which indicated light-on vs light-off for BR-D96N at pH 10.5, was measured at 63 mV. We were unable to measure the surface potential difference between light-on and light-off for WT-BR at pH 7.3, most likely because it was not possible to generate enough of the transient M intermediate at pH 7.3 to register a measurable voltage change by SSPM (i.e., the M state did not accumulate in concentrations high enough to be detected by this method). At neutral pH in the WT protein, M-state decay is not inhibited by a lack of protons and, therefore, will not build up in significant steady-state concentrations; because the technique requires the generation of a photosteady-state concentration of M, the resulting light-on − light-off voltage difference was too small to be determined. As the pH of WT-BR was increased, the potential difference between light-on and light-off became measurable (37 mV). The BR mutant D96N, which has a longer M state lifetime, produced a larger potential difference (48 mV) at pH 7.3 compared with WT-BR at

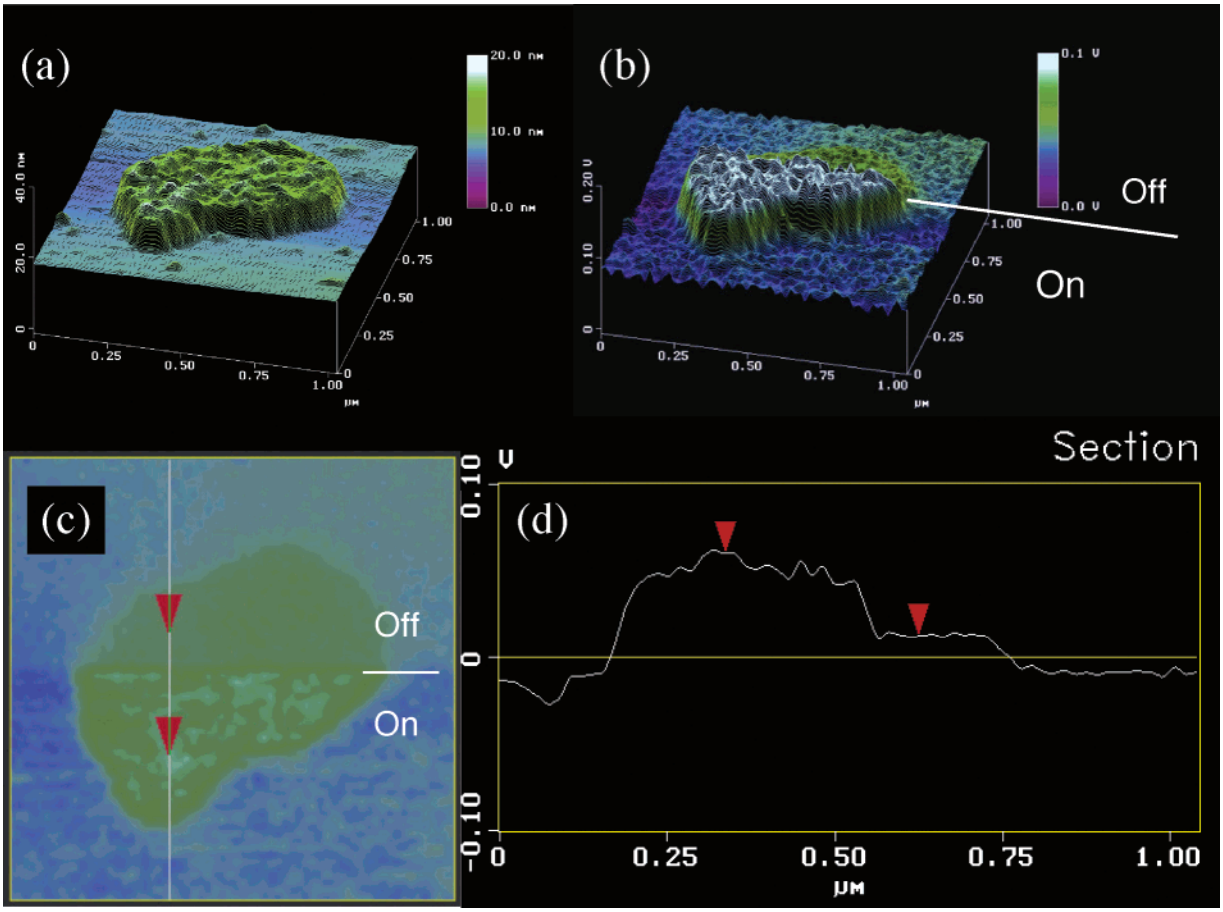

Figure 5. BR D96N at pH 7.3: (a) AFM topographic image, (b) corresponding SSPM surface potential image, and (d) surface potential at the cross section indicated in (c). In graph (d), the 0 μm is at the bottom of the graph (c) and that is light-on on mica. The first pointer is at light-on on BR D96N, and the second pointer is at light-off on BR D96N. The potential then falls to ~0 V (at around 0.75 μm mark) on light-off mica surface. The vertical distance between the two pointers, which corresponds to the surface potential difference between light on and light off for BR D96N at pH 7.3, was 48 mV.

pH 7.3. A larger potential difference (63 mV) could be obtained on BR-D96N as the pH was increased to 10.5. The potential difference between light-on and light-off of BR-D96N is almost twice the value of WT-BR, both at pH 10.5. Many molecules, such as oriented liquid water form icelike structure on surface[58] and natural organic matter (humic substances),[59] tend to adsorb to mica due to its very active surface properties. Because it is possible that unknown molecules may adsorb on the mica substrate, the potential difference between the substrate and the BR may vary from sample to sample due to different adsorbates. Although we observed approximately zero surface potential on the mica substrate for all samples while the incident light was on or off, we do not believe the potential differences between the mica surface and the BR membrane (both light on and light off) are reliable data. Thus, the surface potential measurements in this study are light-on BR potential versus light-off BR potential. Our results were consistent with previous studies that the total charge on the extracellular side of the membrane was balanced, with no obvious structural distribution of positive or negative charges.[32] When the light was on, the surface potentials were generated from net surface charge densities on the BR membrane surface. The theoretical potential distribution and field for a hyperboloidal probe in a uniform field, generated by a surface charge density σ, have been calculated previously.[60] The partial surface potential $\Phi_i(r)$ due to the surface charge density σ was:

$$\Phi_i(r) = (4\pi\sigma z_0)\int_1^{\infty} \varphi_{q,j}(\eta,\eta',\mu)\eta' \mathrm{d}\eta'$$

where the z_0 is the distance between the probe and the sample surface, and $\varphi_{q,j}$ (η,η',μ) is a continuous function describing the tip shape in Spheroidal coordinate. It indicates that a surface charge density generation and a longer lifetime would produce a larger surface potential than is measurable by SSPM.

To understand the molecular origins of the signals observed in BR and D96N, we generated an electrostatic difference map associated with the formation of the late M state in D96N. This intermediate has been studied using X-ray crystallography, and this study also provided coordinates for the resting state.[26] By adding and minimizing the hydrogen atoms, we can calculate the atomic charges using semiempirical molecular orbital theory (see Theory and Modeling). An electrostatic difference map was generated by orienting the two structures to maximal overlap of the backbone atoms and subtracting the resting-state field from the late M-state field. The result is shown in Figure 7. The lines are drawn for a plane that runs parallel to the proton channel as defined by Asn-96 (residue centroid), the nitrogen atom of the chromophore, and a point equidistant from the four carbonyl or carboxylate oxygens of Glu-194 and Glu-204. Note that a proton is not pumped across the membrane in our simulation. The only proton motion involves residues within the binding site, as noted below.

The extracellular surface becomes significantly more positive in the late M state relative to the BR-like resting state of D96N.

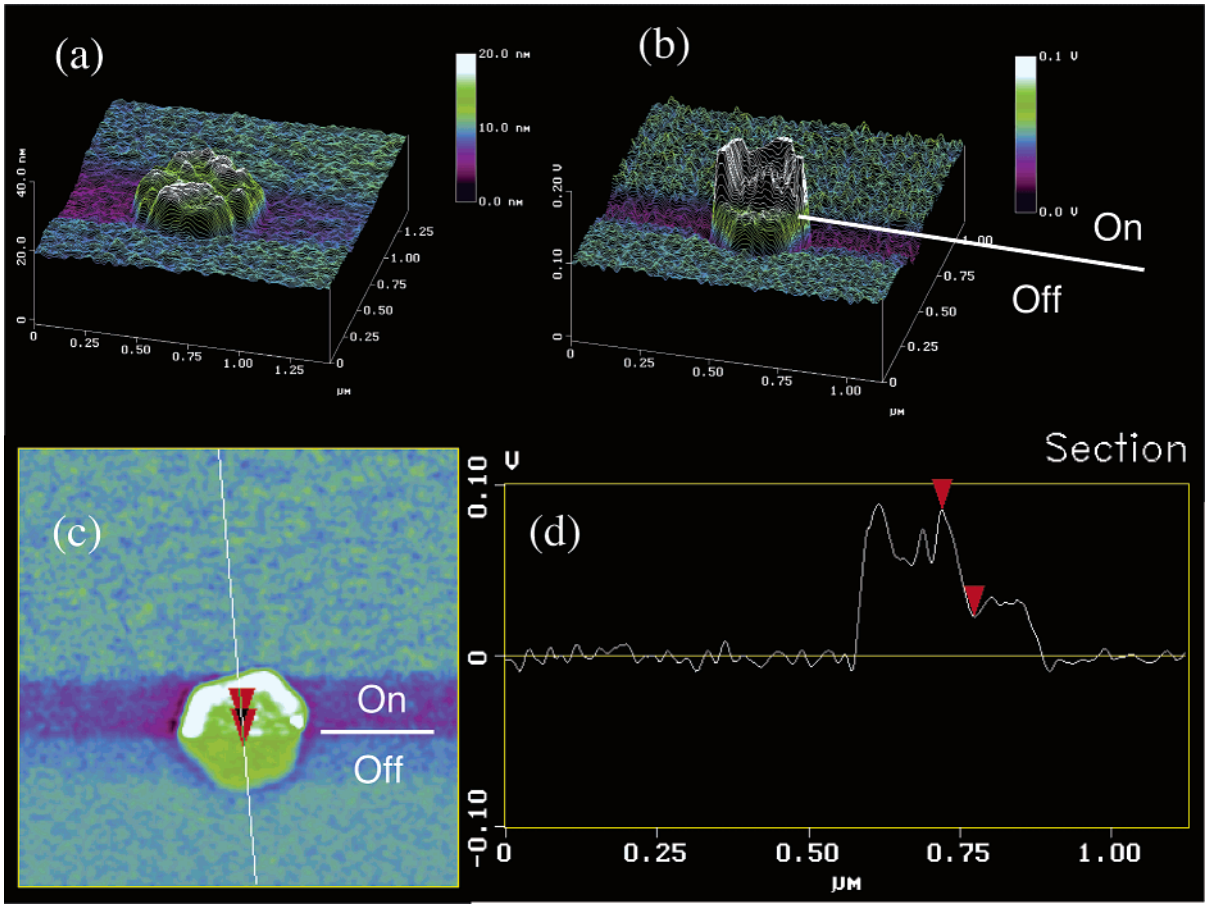

Figure 6. BR D96N at pH 10.5: (a) AFM topographic image, (b) corresponding SSPM surface potential image, and (d) surface potential at the cross section indicated in (c). In graph (d), the 0 μm is at the top of the graph (c) and is light-on on mica (~0 V). The first pointer is at light-on on BR D96N, and the second pointer is at light-off on BR D96N. The potential then falls to ~0 V (at around 0.9 μm mark) on light-off mica surface. The vertical distance between the two pointers, which corresponds to the surface potential difference between light on and light off for BR D96N at pH 10.5, was 63 mV.

The shift in charge is equivalent to a dipole moment change of 31.5 D (see Figure 7). The two primary molecular events responsible for this dramatic change in field are summarized in Figure 7. First, a proton is transferred from the chromophore nitrogen to Asp-85, making both the chromophore and this Asp residue neutral. This proton shift generates a net shift in positive charge toward the extracellular side. Of equal importance is the shift of the positively charged Arg-82 (arginine 82) from a position facing up into the binding site to a conformation in which this residue is aimed down toward the extracellular surface. There has long been experimental and theoretical evidence in support of the Arg-82 residue shifting down during the latter stages of the BR photocycle.[61−63] The crystallography studies of Luecke et al. indicate that this process is complete in the late M state of D96N,[26] although molecular dynamics simulations suggest it may take place during the M to N transition in the wild-type protein.[57] The motion of Arg-82 accounts for about 25% of the total electrostatic shift observed at the extracellular surface.

We ran calculations with and without water and noticed no significant changes in the fields at the surfaces, but significant differences in the microstructure of the fields within the protein. The water molecules enhance field discontinuities and are responsible for most of the abrupt changes in the field. However, these changes are damped out by distance. The net effect is that the water molecules orient in the field induced by the transfer of a proton to Asp-85 and the conformational flip of Arg-82 and in the process enhance and stabilize the field. Water reorientation is responsible for approximately 30% of the field observed at the extracellular surface.

The photovoltaic observations reported herein provide the opportunity to propose a mechanistic basis for the B2 component of the photovoltage. As reported previously, reorientation of the Arg-82 amidinium group is believed to play a pivotal role in B1.[31] During the M state, further repositioning of this group occurs in the opposite direction (i.e., away from the chromophore and primary counterions toward the extracellular surface and the proton release group). To produce the data presented in Figures 3−5, a photosteady-state population of the M state was required. Wild-type protein at neutral pH responded faster than the detection limits of the technique, so the M state was examined by resorting to high pH samples and the D96N mutant. As stated above, high pH retards M-state decay in both the wild type and D96N proteins, allowing facile generation of large steady-state populations of the intermediate. The magnitude of the resulting SSPM signals is proportional to the M-state population in each sample. Furthermore, the nature of the SSPM signals is consistent with both Arg-82 reorientation and the B1 to B2 transition—from a fast negative photovoltage spike to a slower increasing signal of opposite polarity. This corresponds nicely to the predicted movements of the Arg-82 amidinium group, toward both Asp-85 and the retinal chromophore during K formation (B1), followed by movement in an opposite direction during the M state (B2). Therefore, the SSPM signals derived from both high pH wild type BR and the mutant D96N essentially represent a steady-state measurement of B2.

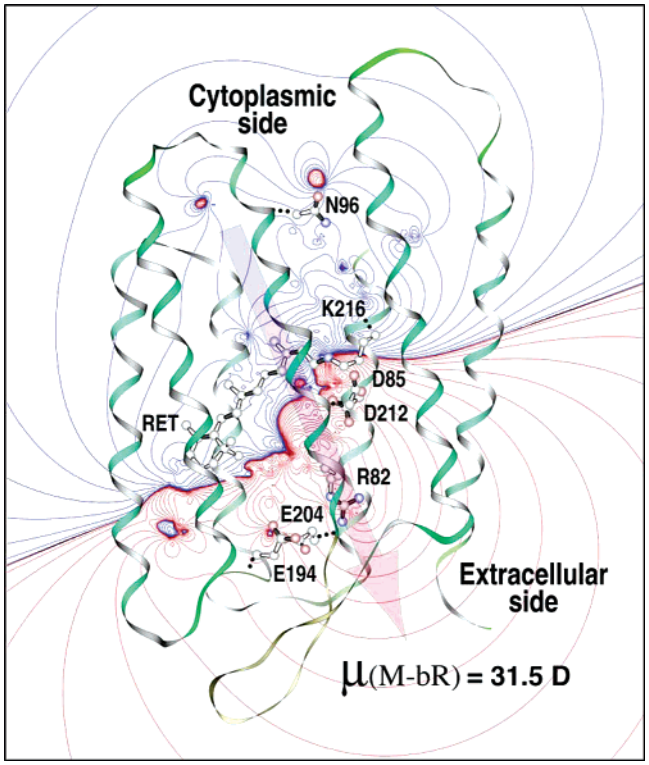

Figure 7. Electrostatic contours associated with the formation of the late M state relative to the BR-like resting state in the mutant D96N on the basis of the diffraction experiments of ref 26. Red contours represent regions where the positive charge has increased, and blue contours represent regions where the negative charge has increased upon formation of the late M state. Contour levels are drawn at the following energies: 0 (black), ±1, ±6, ±19, ±45, ±88, ±152, ±241, ±359, ±511, ±702, ±934, ±1212, ±1541, ±1925, ±2368, ±2874, ±3447, ±4092, ±4812, ±5613 J/mol. These numbers should be divided by the dielectric constant, which was assumed to be unity for the purposes of calculating the electrostatic energies.

We have demonstrated direct measurements of photoinduced surface potential on WT-BR and BR-D96N at various pH values by SSPM. At a relatively high humidity of 65−70%, the BR membranes retained their photoactivty and the surface potential differences between light-on and light-off were measured. The potential difference increased as the pH increased in both WT-BR and BR-D96N. The light-induced potential difference was also higher in the BR-D96N membrane than in WT-BR at the same pH. We conclude that the origin of the surface potentials was the generation of surface charge on the extracellular side of the membrane. A higher surface potential correlated with a longer lifetime of these charges. Possible applications of the observed photoinduced potential change of the BR and D96N proteins include optical coupled FETs, high-speed photodetectors and artificial retinas.

Acknowledgment. This research was supported by the Office of Basic Energy Sciences, U.S. Department of Energy (I.L., E.G.). Oak Ridge National Laboratory is managed by UT-Battelle, LLC, for the U.S. Department of Energy, under Contract No. DE-AC05-00OR22725. This research was also supported in part by grants NSF 0412387 and 0432151 (J.A.S., R.R.B.) and NIH GM-34548 (R.R.B.).

References and Notes

(1) Grigorieff, N.; Ceska, T. A.; Downing, K. H.; Baldwin, J. M.; Henderson, R. *J. Mol. Biol.* **1996**, *259*, 393.
(2) Gillespie, N. B.; Wise, K. J.; Ren, L.; Stuart, J. A.; Marcy, D. L.; Hillebrecht, J.; Li, Q.; Ramos, L.; Jordan, K.; Fyvie, S.; Birge, R. R. *J. Phys. Chem. B* **2002**, *106*, 13352.
(3) Lanyi, J. K.; Varo, G. *Isr. J. Chem.* **1995**, *35*, 365.
(4) Birge, R. R.; Gillespie, N. B.; Izaguirre, E. W.; Kusnetzow, A.; Lawrence, A. F.; Singh, D.; Song, Q. W.; Schmidt, E.; Stuart, J. A.; Seetharaman, S.; Wise, K. J. *J. Phys. Chem. B* **1999**, *103*, 10746.
(5) Butt, H. J.; Fendler, K.; Bamberg, E,; Tittor, J.; Oesterhelt, D. *EMBO* **1989**, *8*, 1657.
(6) Hampp, N.; Popp, A.; Bräuchle, C.; Oesterhelt, D. *J. Phys. Chem. B* **1992**, *96*, 4679.
(7) Hampp, N.; Bräuchle, C.; Oesterhelt, D. *MRS Bull.* **1992**, *17*, 56.
(8) Oesterhelt, D.; Bräuchle, C.; Hampp, N. *Quart. Rev. Biophys.* **1991**, *24*, 425.
(9) Sass, H. J.; Schachowa, I. W.; Rapp, G.; Koch, M. H.; Oesterhelt, D.; Dencher, N. A.; Buldt, G. *EMBO* **1997**, *16*, 1484.
(10) Luecke, H.; Schobert, B.; Richter, H.-T.; Cartailler, J.-P.; Lanyi, J. K. *Science* **1999**, *286*, 255.
(11) Sass, H. J.; Buldt, G.; Gessenich, R.; Hehn, D.; Neff, D.; Schlesinger, R.; Berendzen, J.; Ormos, P. *Nature* **2000**, *406*, 649.
(12) Ludmann, K.; Gergely, C.; Der, A.; Varo, G. *Biophys. J.* **1998**, *75*, 3120.
(13) Lanyi, J. K.; Schobert, B. *J. Mol. Biol.* **2003**, *328*, 439.
(14) Sass, H. J.; Gessenich, R.; Koch, M. H.; Oesterhelt, D.; Dencher, N. A.; Buldt, G.; Rapp, G. *Biophys. J.* **1998**, *75*, 399.
(15) Radionov, A. N.; Kaulen, A. D. *FEBS Lett.* **1997**, *409*, 137.
(16) Lanyi, J.; Schobert, B. *J. Mol. Biol.* **2002**, *321*, 727.
(17) Schobert, B.; Brown, L. S.; Lanyi, J. K. *J. Mol. Biol.* **2003**, *330*, 553.
(18) Onufriev, A.; Smondyrev, A.; Bashford, D. *J. Mol. Biol.* **2003**, *332*, 1183.
(19) Kandt, C.; Schlitter, J.; Gerwert, K. *Biophys. J.* **2004**, *86*, 705.
(20) Spazzov, V. Z.; Luecke, H.; Gerwert, K.; Bashford, D. *J. Mol. Biol.* **2001**, *312*, 203.
(21) Garczarek, F.; Wang, J.; El-Sayed, M. A.; Gerwert, K. *Biophys. J.* **2004**, *87*, 2676.
(22) Garczarek, F.; Brown, L. S.; Lanyi, J. K.; Gerwert, K. *Proc. Natl. Acad. Sci. U.S.A.* **2005**, *102*, 3633.
(23) Luecke, H.; Richter, H. T.; Lanyi, J. K. *Science* **1998**, *280*, 1934.
(24) Weik, M.; Zaccai, G.; Dencher, N. A.; Oesterhelt, D.; Hauss, T. *J. Mol. Biol.* **1998**, *275*, 625.
(25) Dickopf, S.; Heyn, M. P. *Biophys. J.* **1997**, *73*, 3171.
(26) Luecke, H.; Schobert, B.; Richter, H.-T.; Cartailler, J.-P.; Lanyi, J. K. *J. Mol. Biol.* **1999**. *291*, 899.
(27) Luecke, H.; Schobert, B.; Cartailler, J.-P.; Richter, H.-T.; Rosengarth, A.; Needleman, R.; Lanyi, J. K. *J. Mol. Biol.* **2000**, *300*, 1237.
(28) Liu, S. Y. *Biophys. J.* **1990**, *57*, 943.
(29) Butt, H. J.; Fendler, K.; Bamberg, E.; Tittor, J.; Oesterhelt, D. *EMBO J.* **1989**, *8*, 1657.
(30) Wang, J.-P.; Song, L.; Yoo, S.-K.; El-Sayed, M. A. *J. Phys. Chem. B* **1997**, *101*, 10599.
(31) Xu, J.; Stickrath, A. B.; Bhattacharya, P.; Nees J.; Varo, G.; Hillebrecht, J. R.; Ren, L.; Birge, R. R. *Biophys. J.* **2003**, *85*, 1128.
(32) Kimura, Y.; Vassylyev, D. G.; Miyazawa, A.; Kidera, A.; Matsushima, M.; Mitsuoka, K.; Murata, K.; Hirai, T.; Fujiyoshi, Y. *Nature* **1997**, *389*, 206.
(33) Genick, U. K.; Soltis, S. M.; Kuhn, P.; Canestrelli I. L.; Getzoff E. D.; *Nature* **1998**, *392*, 206.
(34) Schobert, B.; Cupp-Vickery, J.; Hornak, V.; Smith, S. O.; Lanyi, J. K. *J. Mol. Biol.* **2002**, *321*, 715.
(35) Hartley, P.; Matsumoto, M.; Mulvaney, P. *Langmuir* **1998**, *14*, 5203.
(36) Nonnenmacher, M.; O'boyle, M.; Wickramsinghe, H. K. *Appl. Phys. Lett.* **1991**, *58*, 2921.
(37) Yokoyama, H.; Inoue, T. *Mol. Thin Solid Films* **1994**, *242*, 33.
(38) Fujihara, M.; Kawate, H.; Yasutake, M. *Chem. Lett.* **1992**, *11*, 2223.
(39) Sakomura, M.; Oono, T.; Sakon, R.; Fujihira, M. *Ultramicroscopy* **2002**, *91*, 215.
(40) Lee, I.; Lee, J. W.; Stubna, A.; Greenbaum, E. *J. Phys. Chem. B* **2000**, *104*, 2439.
(41) Bluhm, H.; Inoue, T.; Salmeron, M. *Surf. Sci.* **2000**, *462*, L599.
(42) Lee, I.; Justus, B. L.; Lee, J. W.; Greenbaum, E. *J. Phys. Chem. B* **2003**, *107*, 14225.
(43) Maslova, M. V.; Gerasimova, L. G.; Forsling, W. *Colloid J.* **2004**, *66*, 364.
(44) Muller, D. J.; Amrein, M.; Engel, A. *J. Struct. Biol.* **1997**, *119*, 172.
(45) Fisher, K. A.; Yanagimoto, K. *J. Cell Biol.* **1978**, *77*, 611.
(46) Muller, D. J.; Schoenenberger, C.; Buldt, G.; Engel, A. *Biophys. J.* **1996**, *70*, 1796.
(47) Sass, H. J.; Buldt, G.; Gessenich, R.; Hehn, D; Neff, D.; Schlesinger, R.; Berendzen, J.; Ormos, P. *Nature* **2000**, *406*, 649.
(48) Lanyi, J. K.; Luecke, H. *Curr. Opin. Struct. Biol.* **2001**, *11*, 415.

(49) Spassov, V. Z.; Luecke, H.; Gerwert, K.; Bashford, D. *J. Mol. Biol.* **2001**, *312*, 203.
(50) Lanyi, J.; Schobert, B. *J. Mol. Biol.* **2002**, *321*, 727.
(51) Luecke, H.; Schobert, B.; Cartailler, J.-P.; Richter, H.-T.; Rosengarth, A.; Needleman, R.; Lanyi, J. K. *J. Mol. Biol*. **2000**, *300*, 1237.
(52) Baudry, J.; Tajkhorshid, E.; Molnar, F.; Phillips, J.; Schulten, K. *J. Phys. Chem. B* **2001**, *105*, 905.
(53) Jacobs, H. O.; Leuchtmann, P.; Homan, O. J.; Stemmer, A. *J. Appl. Phys.* **1998**, *84*, 1168.
(54) Stewart, J. J. P. *MOPAC 2000 Manual*; Fujitsu Limited, 1999.
(55) Ren, L.; Martin, C. H.; Wise, K. J.; Gillespie, N. B.; Luecke, H.; Lanyi, J. K.; Spudich, J. L.; Birge, R. R. *Biochemistry* **2001**, *40*, 13906.
(56) Hehre, W. J.; Yu, J.; Klunzinger, P. E.; Lou, L. *A Brief Guide to Molecular Mechanics and Quantum Chemical Calculations*; Wavefunction, Inc.: Irvine, CA, 1998.
(57) Kusnetzow, A.; Dukkipati, A.; Babu, K. R.; Singh, D.; Vought, B. W.; Knox, B. E.; Birge, R. R. *Biochemistry* **2001**, *40*, 7832.
(58) Odelius, M.; Bernasconi, M.; Parrinello, M. *Phys. Rev. Lett*. **1997**, *78*, 2855.
(59) Maurice, P. A.; Namjesnik-Dejanovic, K. *Environ. Sci. Technol*. **1999**, *33*, 1538.
(60) Passian, A.; Wig, A.; Meriaudeau, F.; Ferrell, T. L. *J. Vac. Sci. Technol., B* **2002**, *20*, 76.
(61) Balashov, S.; Govindjee, R.; Kono, M.; Imasheva, E.; Lukashev, E.; Ebrey, T.; Crouch, R.; Menick, D.; Feng, Y. *Biochemistry* **1993**, *32*, 10331.
(62) Kusnetzow, A.; Singh, D. L.; Martin, C. H.; Barani, I.; Birge, R. R. *Biophys. J.* **1999**, *76*, 2370.
(63) Hutson, M. S.; Alexiev, U.; Shilov, S. V.; Wise, K. J.; Braiman, M. S. *Biochemistry* **2000**, *39*, 13189.